Pyrene-Functionalized Ruthenium Nanoparticles: Novel Fluorescence Characteristics from Intraparticle Extended Conjugation

Wei Chen, Nathaniel B. Zuckerman, James W. Lewis, Joseph P. Konopelski, and Shaowei Chen*

Department of Chemistry and Biochemistry, University of California, 1156 High Street, Santa Cruz, California 95064

Received: July 20, 2009; Revised Manuscript Received: August 8, 2009

Ruthenium nanoparticles functionalized with pyrene moieties were prepared by olefin metathesis reactions of carbene-stabilized nanoparticles with 1-vinylpyrene and 1-allylpyrene (referred to as Ru═VPy and Ru═APy, respectively). ^{1}H NMR spectroscopic measurements showed that the surface concentration of the pyrene moieties was 26.4 and 22.9%, respectively. In fluorescence measurements, Ru═VPy nanoparticles exhibited two prominent emission bands at 392 and 490 nm, very similar to those of (*E*)-1,2-di(pyren-1-yl)ethene, suggesting that the particle-bound pyrene moieties might behave equivalently to pyrene dimers with a conjugated linker by virtue of the Ru═carbene π bonds. In sharp contrast, Ru═APy nanoparticles displayed only a single emission peak at 392 nm, consistent with monomeric pyrene derivatives of 1-vinylpyrene and 1-allylpyrene. This implies that the intraparticle extended conjugation might be effectively turned off by the insertion of an sp^3 carbon into the chemical linker that bound the pyrene moieties onto the nanoparticles. In addition, Ru═VPy nanoparticles exhibited a rather long lifetime of the emission at 490 nm, as compared to that of the conjugated pyrene dimer, suggesting that the nanoparticles might be less prone to photobleaching. This is attributed to the neighboring organic protecting ligands that may create a more rigid chemical environment for the nanoparticle-bound pyrene moieties and thus prolong the life of the excited state, as compared to the strong electrostatic perturbations which exist in free solution when surrounded by a polar solvent.

Introduction

Monolayer protected nanoparticles represent a unique class of nanomaterials in that the materials properties may be readily manipulated by the structures and bonding interactions of the metal core and the organic protecting layers. For instance, whereas mercapto derivatives have been used as the ligands of choice in the preparation of a number of nanoparticle materials by virtue of the strong affinity of the thiol groups to transition metal surfaces,[1−3] the effects of the interfacial bonding interactions on the nanoparticle materials properties have been largely ignored primarily because of the lack of interesting chemistry of the metal−thiol bonds. However, several recent studies[4−9] have shown that nanoparticles may also be passivated by metal−carbon covalent bonds, which play an important role in the manipulation of the optoelectronic properties of the resulting particle materials. For instance, metal nanoparticles stabilized by metal−carbene π bonds have been found to exhibit apparent intraparticle charge delocalization,[8,9] equivalent to the formation of an extended conjugation system between the particle-bound functional moieties. This has recently been exemplified by the intervalence charge transfer between ferrocenyl moieties bound to ruthenium nanoparticle and thin film surfaces through Ru═C π bonds,[9,10] confirming Hush's four-decade-old prediction.[11]

It is envisioned that such a fundamental mechanism may be exploited to manipulate the optical properties of nanoparticle materials as well. Note that the aforementioned nanoparticles have been known to serve as a nanoscale structural scaffold where multiple functional moieties can be readily incorporated into the nanoparticle protecting shell by ligand place exchange reactions and/or surface coupling reactions.[1−3,8,9] For instance, various fluorophores have been used for the chemical decoration of nanoparticle molecules where an understanding of the photoinduced electron and energy transfer may offer fundamental insights of the photochemical and photophysical properties of functional moieties bound onto nanoparticle surfaces, a critical part of nanoparticle-based photovoltaics and of biomolecular labeling and detection.[12−15] However, in most of these earlier studies, the fluorophores were immobilized onto the nanoparticle surface by thiols, amines, and isocyanates and/or with an aliphatic linker,[16−20] where the optical characteristics of the nanoparticles are largely the simple summation of those of individual fluorophore moieties. In other words, the fluorophores typically behave independently because of a lack of electronic interactions.

In the present study, we demonstrate that when fluorophores are bound onto the nanoparticle surface through metal−carbene π bonds, the resulting intraparticle charge delocalization provides an extended conjugation platform where novel optical behaviors emerge, in sharp contrast to early studies with mostly localized interfacial bonding interactions. We use carbene-stabilized ruthenium nanoparticles as the illustrating example, which are functionalized by varied pyrene derivatives through olefin metathesis reactions. Pyrene and its derivatives have been used extensively as sensitive fluorescence probes for neutral organic compounds and inorganic anions.[21−25] We observe that when pyrene moieties are bound onto the ruthenium nanoparticle surface directly by Ru═C π bonds, as exemplified by metathesis reactions of carbene-stabilized ruthenium nanoparticles with vinylpyrene, fluorescence measurements exhibit a new emission peak in the visible range, consistent with pyrene dimers bridged

* To whom correspondence should be addressed. E-mail: schen@chemistry.ucsc.edu.

10.1021/jp906874f CCC: $40.75
Published on Web 09/02/2009

SCHEME 1: Chemical Structures of Pyrene Derivatives

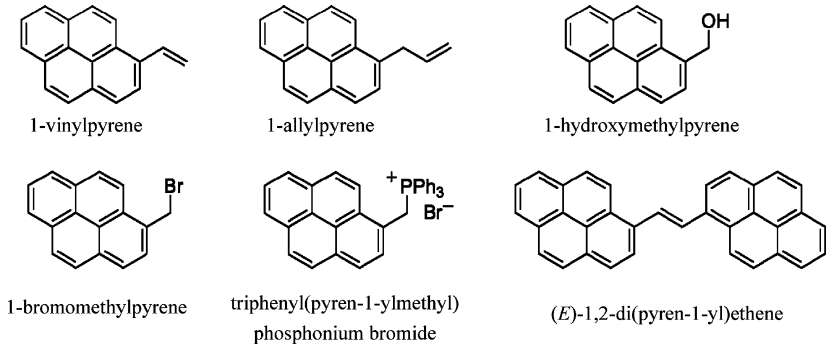

1-vinylpyrene | 1-allylpyrene | 1-hydroxymethylpyrene

1-bromomethylpyrene | triphenyl(pyren-1-ylmethyl) phosphonium bromide | (*E*)-1,2-di(pyren-1-yl)ethene

by a conjugated spacer and in sharp contrast to the fluorescence properties of monomeric pyrene which typically emits in the near UV region. In essence, the conjugated interfacial bonding interactions provide an effective mechanism for intraparticle electronic interactions. Interestingly, this may be effectively turned off by the insertion of a saturated methylene spacer into the chemical linkage, as manifested by the control experiment with allylpyrene. These results offer a rare glimpse of the molecular control of the optical characteristics of fluorophore-functionalized nanoparticles where the metal−ligand interfacial bonding interactions play a critical role, a fundamental property that may find applications in diverse areas such as optoelectronics, chemical sensing, photocatalysis, and photovoltaics.

Experimental Section

Chemicals. Ruthenium chloride ($RuCl_3$, 99+%, ACROS), 1,2-propanediol (ACROS), sodium acetate trihydrate ($NaAc \cdot 3H_2O$, MC&B), and extra dry *N*,*N*-dimethylformamide (DMF, 99.8%, Aldrich) were used as received. All other chemicals and solvents were obtained from typical commercial sources and were used without further treatment unless otherwise specified. Water was supplied by a Barnstead Nanopure water system (18.3 MΩ·cm).

Syntheses of Pyrene Derivatives (Scheme 1). The synthetic procedures reported in the literature were adopted for the preparation of 1-vinylpyrene,[26] 1-allylpyrene,[27] 1-hydroxymethylpyrene,[28] 1-bromomethylpyrene,[28] triphenyl(pyren-1-ylmethyl)phosphonium bromide,[29] and (*E*)-1,2-di(pyren-1-yl)-ethene.[29] The details are included in the Supporting Information, along with the data of spectroscopic characterizations. Experimentally, standard syringe techniques using flame and/or oven-dried glassware were utilized for the syntheses under an atmosphere of nitrogen. All melting points were uncorrected. Proton NMR measurements were run in the specified deuterated solvents at 500 or 600 MHz, while carbon NMR spectra were acquired at 125 MHz. The chemical shifts were reported in parts per million (ppm), and ^1H and ^{13}C spectra were calibrated against residual solvent peaks as follows: $CDCl_3$ (7.26, 77.2 ppm) and CD_3OD (3.31, 49.0 ppm). Anhydrous THF, toluene, and CH_2Cl_2 were obtained from a solvent purification system. Diethyl ether and benzene were refluxed over sodium metal and benzophenone ketyl radical prior to distillation. Pyridine was distilled over sodium hydroxide and stored over 4 Å molecular sieves. Potassium *tert*-butoxide was sublimed freshly before use. Allyl bromide was washed with $NaHCO_3$ and water, dried with $MgSO_4$, and distilled freshly before use. Triphenylphosphine was recrystallized from hexanes and dried under a vacuum for 24 h over P_2O_5. *n*-BuLi in hexanes was titrated with diphenylacetic acid. All other solvents and reagents were used as received unless otherwise noted. Flash chromatography was performed using Flash grade, 60 Å silica with mixtures of HPLC grade ethyl acetate/hexanes as eluent unless otherwise noted. Thin layer chromatography (TLC) was performed using UV silica plates for determining reaction progress and flash chromatography gradients.

Preparation of Pyrene-Functionalized Ruthenium Nanoparticles. First, carbene-stabilized ruthenium nanoparticles were prepared by taking advantage of the strong affinity of the diazo functional group to ruthenium surfaces. Experimentally, octyl diazoacetate (ODA) ligands were mixed with Ru nanoparticles that were freshly prepared by thermolytic reduction of ruthenium chloride in 1,2-propanediol.[8] The resulting purified nanoparticles were denoted as Ru═C8, which exhibited a core diameter of 2.12 ± 0.72 nm, as determined by transmission electron microscopy (TEM) measurements.

Pyrene-functionalized Ru nanoparticles were then prepared by olefin metathesis reactions of the Ru═C8 particles obtained above with vinyl-terminated pyrene derivatives (Scheme 2). In a typical reaction, Ru═C8 and vinylpyrene (the molar ratio of vinylpyrene to particle-bound carbene ligands was 3:1) were dissolved in dichloromethane (DCM) under magnetic stirring for 3 days. The solution was then dried, and the sample was washed with ethanol to remove excessive vinylpyrene and displaced ligands. The purified particles were referred to as Ru═VPy. Metathesis reactions of the Ru═C8 particles with allylpyrene were carried out in a similar fashion and the resulting particles were denoted as Ru═APy.

Spectroscopies. UV−vis spectroscopic studies were performed with an ATI Unicam UV4 spectrometer using a 1 cm quartz cuvette with a resolution of 2 nm. The surface concentration of the pyrene moieties was evaluated by proton nuclear magnetic resonance (^1H NMR) spectroscopy (Varian Unity 500 MHz). Experimentally, the metal cores of Ru nanoparticles were dissolved by dilute potassium cyanide (KCN) before the ^1H NMR spectra of the remaining organic components were acquired. Fluorescence spectra were acquired with a PTI fluorescence spectrometer. Fourier transform infrared (FTIR) measurements were carried out with a Perkin-Elmer FTIR spectrometer (Spectrum One) where the samples were prepared by casting a particle solution onto a NaCl disk. The spectral resolution was 4 cm^{-1}.

Fluorescence Lifetime Measurements. Nanosecond time-resolved fluorescence spectra were acquired by exciting the particle solutions with 7 ns pulses of 355 nm light from the third harmonic of a Q-switched Nd:YAG laser (QuantaRay DCR-2). The excitation fluence was 100 $\mu J/mm^2$, delivered to a 1 mm high strip at the bottom of a 2 mm path length fluorescence cuvette. Emitted light was collected at 90° to the excitation direction using a cutoff filter (Schott OG-370) to eliminate Rayleigh scattered laser light. Photoluminescence was

SCHEME 2: Olefin Metathesis Reactions of Carbene-Stabilized Ruthenium Nanoparticles with Vinylpyrene

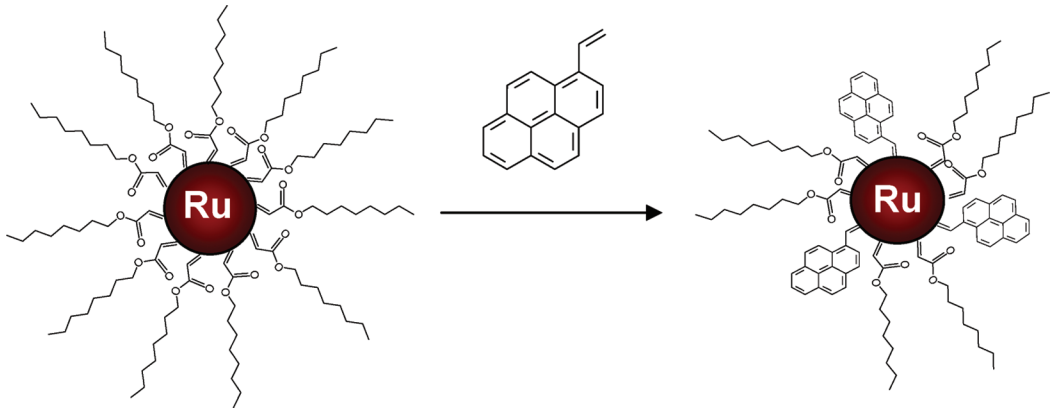

dispersed in a spectrograph (Jarrell-Ash MonoSpec 27 whose entrance slit was 500 μm and whose holographic grating had 150 grooves/mm) with the light finally detected by an Andor DH520 intensified charge coupled device (ICCD) detector whose intensifier photocathode had an extended red S-20 response.

Emitted light was detected using a series of intensifier gate widths, with the start of the gate pulse always positioned 15 ns after the peak of the laser pulse (as determined by the peak detected intensity at 355 nm from a scattering sample with neutral density filters replacing the cutoff filter). Gate widths were 5, 10, 20, 40, 80, and 160 ns and were controlled by a Stanford Research Systems DG-535 digital delay generator. Under these conditions, the emitted light (I_f, detected for a given gate width Δt and wavelength λ) should be described by the relationship

$$I_f(\lambda, \Delta t) = I_{f,t>15\,ns}(\lambda)[1 - I_1(\lambda)e^{-\Delta t/\tau_1} ...] \quad (1)$$

where $I_{f,t>15\,ns}(\lambda)$ is the total photoluminescence detected for times longer than 15 ns after the peak of the laser pulse, $I_1(\lambda)$ is the wavelength distribution of photoluminescence decaying with time constant τ_1, and "..." expresses the possibility of photoluminescence decaying with more than one time constant. Data were fit globally using Matlab routines previously developed to fit time-resolved absorbance changes.[30,31]

Results and Discussion

As mentioned earlier, the pyrene moieties were incorporated into the nanoparticle protecting shell by metathesis reactions (Scheme 2). The concentration of the pyrene functional groups on the nanoparticle surface was quantitatively evaluated by ^{1}H NMR measurements, where the metal cores were dissolved by dilute KCN and the organic components were extracted for NMR measurements (Figure S1 in the Supporting Information).[9] The peaks within the range 7.8−8.4 ppm were ascribed to the aromatic protons of the pyrene rings, whereas that at 0.9 ppm to methyl protons of the original carbene ligands. From the ratio of the integrated peak areas, the surface concentration of the pyrene moieties on the Ru═VPy and Ru═APy nanoparticles was estimated to be 26.4 and 22.9%, respectively. This suggests that on average there are approximately 20 pyrene functional groups per nanoparticle.[9]

UV−visible absorption measurements were then carried out. Figure 1 depicts the optical absorption spectra of the Ru═C8, Ru═VPy, and Ru═APy nanoparticles, along with those of 1-vinylpyrene and 1-allylpyrene. Both of the pyrene monomers

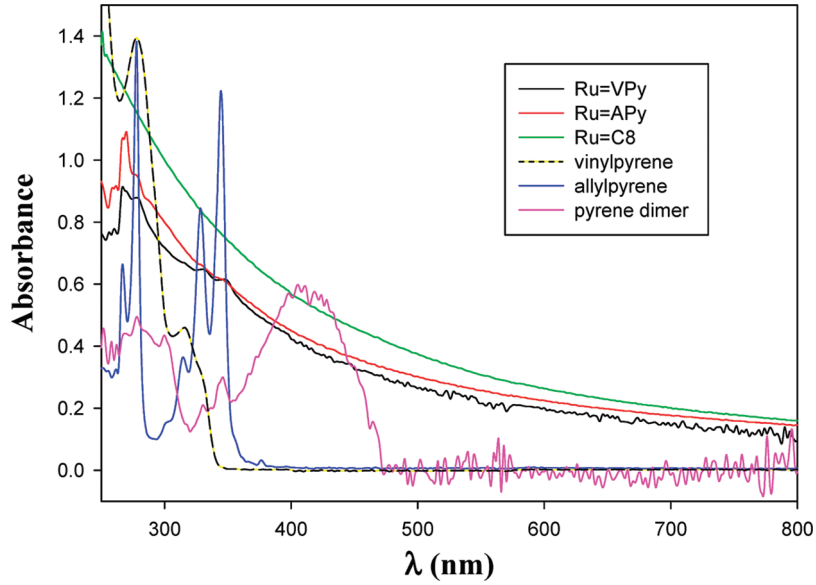

Figure 1. UV−visible spectra of the Ru═C8, Ru═VPy, and Ru═APy nanoparticles, as well as 1-vinylpyrene, 1-allylpyrene, and (*E*)-1,2-di(pyren-1-yl)ethene (i.e., pyrene dimer). The concentrations of nanoparticles were all 0.1 mg/mL in DMF, whereas the solutions of the monomeric pyrene derivatives were all 0.1 mM in DMF.

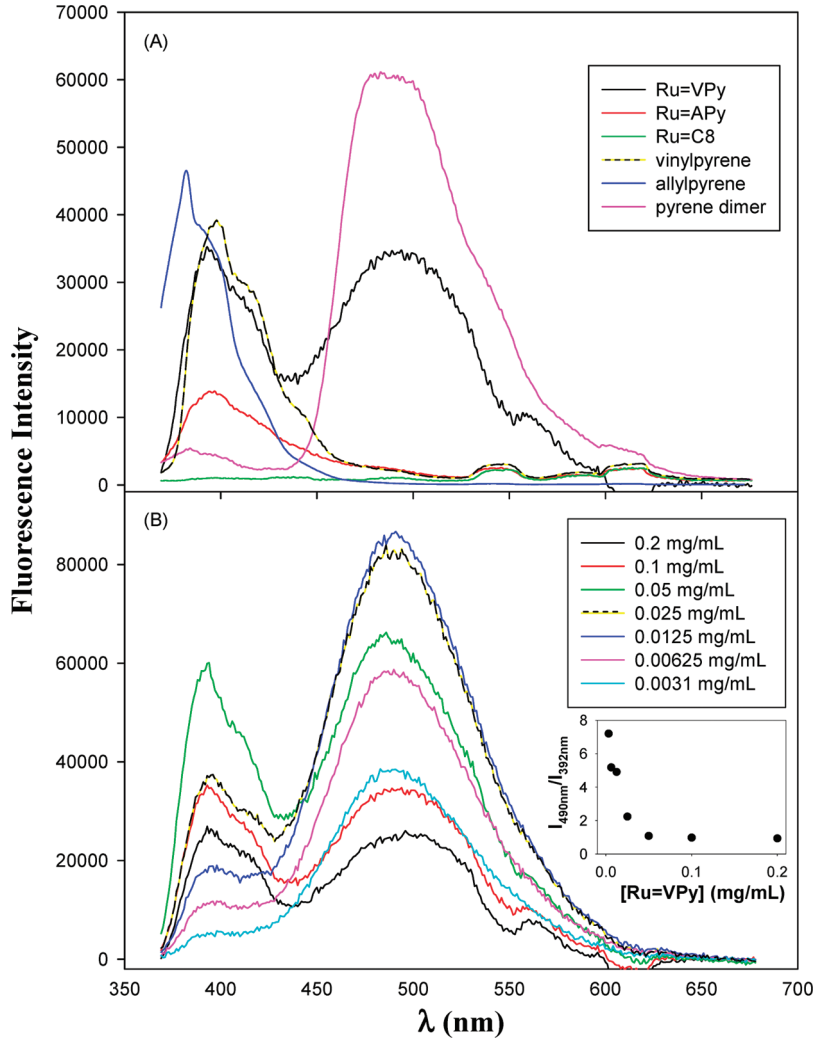

Figure 2. (A) Fluorescence spectra of the Ru═C8, Ru═VPy, and Ru═APy nanoparticles, as well as 1-vinylpyrene, 1-allylpyrene, and (*E*)-1,2-di(pyren-1-yl)ethene (i.e., pyrene dimer). The concentrations of nanoparticles were all 0.1 mg/mL in DMF, whereas the solutions of the monomeric pyrene derivatives were all 0.1 mM in DMF. The small features between 525 and 625 nm were from the solvent background. (B) Fluorescence spectra of Ru═VPy nanoparticles at different concentrations (shown as figure legends) in DMF. The inset shows the variation of the ratio of the intensity of the emission bands at 490 and 392 nm with particle concentration. The excitation wavelength was set at 349 nm for all of the emission spectra.

exhibit very well-defined absorption features below 380 nm. For instance, allylpyrene (blue curve) showed four major absorption peaks at 266, 278, 328, and 344 nm, corresponding to the $\pi-\pi^*$ electronic transitions of the aromatic ring electrons. A similar absorption profile was observed for vinylpyrene (dashed/yellow curve), although the details are somewhat different with two major peaks at 278 and 316 nm (and a shoulder at 328 nm). At longer wavelength, both pyrene derivatives exhibit only featureless responses. For the conjugated pyrene dimer ((*E*)-1,2-di(pyren-1-yl)ethene, magenta curve), however, the absorption features in the UV region diminish, whereas a broad, yet intense peak emerges at ca. 410 nm, most probably as a consequence of the extended conjugation of the aromatic π electrons by the —CH═CH— bridge. For the nanoparticle samples, the absorption characteristics were all very similar, dominated by an exponential decay profile as a result of the Mie scattering of the nanosized Ru cores (green curve).[8] For the Ru═VPy (black curve) and Ru═APy (red curve) nanoparticles, additional features arise in the near UV region (<380 nm) with four apparent absorption peaks at 266−269, 278, 329, and 349 nm. These are attributable to the pyrene moieties on the nanoparticle surfaces, consistent with the aforementioned NMR measurements (Figure S1 in the Supporting Information). The successful incorporation of the pyrene moieties into the nanoparticle protecting layer was further confirmed by FTIR measurements (Figure S2 in the Supporting Information) where the pyrene ring vibrational stretches were very well-defined at 1649 cm^{-1} (Ru═VPy) and 1669 cm^{-1} (Ru═APy). Notably, the somewhat lower vibrational energy for the Ru═VPy nanoparticles might be due to the extended conjugation between particle-bound pyrene moieties by virtue of the Ru═carbene π bonds (more details below).

The pyrene-functionalized nanoparticles prepared above exhibited interesting fluorescence characteristics. As mentioned earlier, pyrene and derivatives are well-known fluorophores that typically emit in the near UV region.[21−25] For instance, as manifested in Figure 2A, when excited at 349 nm, vinylpyrene and allylpyrene show a major emission peak at 398 and 382 nm, respectively (again, the slightly lower energy of the former might be ascribed to the extended conjugation between the vinyl and aromatic ring electrons), each with two additional shoulders at somewhat longer wavelength positions (note that the small features between 525 and 625 nm were from the solvent background). When the pyrene moieties are covalently bound onto the ruthenium nanoparticle surface, the fluorescence characteristics vary drastically with the chemical linkage. From

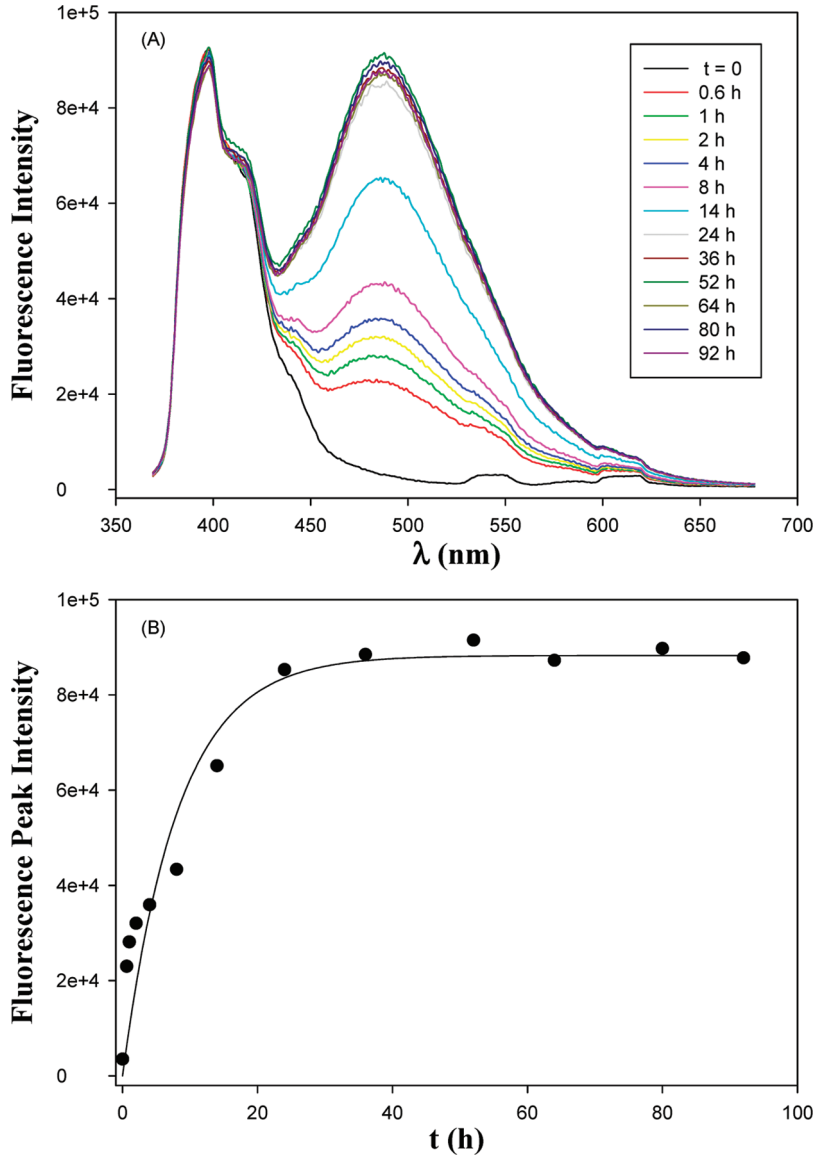

Figure 3. (A) Fluorescence spectra of Ru═C8 nanoparticles mixed with 1-vinylpyrene for different periods of time (shown as figure legends). Ru═C8 concentration, 0.01 mg/mL; vinylpyrene concentration, 3 mM. The excitation wavelength was set at 349 nm. (B) Variation of the fluorescence intensity at 490 nm with reaction time. The symbols are experimental data collected from panel A, and the line is the exponential fit by the equation $y = a(1 - e^{-bx})$, with the fitting parameters $a = -88288$, $b = 0.122$, and $R^2 = 0.92$.

Figure 2A, it can be seen that Ru═VPy nanoparticles displayed two major emission peaks at 392 and 490 nm, in sharp contrast to Ru═APy nanoparticles where a single emission peak appeared at 392 nm and to Ru═C8 nanoparticles where only a featureless profile was observed. Note that the higher energy emission (392 nm) is consistent with the electronic transitions of monomeric pyrene moieties, whereas that at lower energy (490 nm) is in good agreement with that of conjugated pyrene dimers, (*E*)-1,2-di(pyren-1-yl)ethene (magenta curve, which also shows an emission at 384 nm, though much weaker[32]). This strongly suggests that, in Ru═VPy nanoparticles, the pyrene moieties might form an extended conjugation system by virtue of the Ru═C carbene π bonds. That is, because of the conducting nature of the ruthenium nanocores, the particle-bound pyrene moieties might behave equivalently to (*E*)-1,2-di(pyren-1-yl)ethene. Interestingly, the incorporation of sp^3 carbons into the chemical linkage led to an effective turn-off of the intraparticle extended conjugation, as manifested by the Ru═APy nanoparticles. Such a behavior is similar to the nanoparticle-mediated intraparticle intervalence transfer that was observed previously with ferrocene-functionalized ruthenium nanoparticles.[9]

One may note that, in appropriate solvent media and at sufficiently high concentrations (typically >50 μM), pyrene derivatives may form excimers which also exhibit a rather intense emission between 450 and 500 nm.[33,34] The formation of pyrene excimers was also suggested with pyrene-functionalized nanoparticles. For instance, Wang et al.[35] synthesized gold nanoparticles capped with pyrene-terminated long-chain alkanethiols (10-(1-pyrenyl)-6-oxo-decanethiol and 17-(1-pyrenyl)-13-oxo-heptadecanethiol) and found that the intensity of the excimer fluorescence increased with increasing concentration of the gold nanoparticles (from 3×10^{-5} to 1.5×10^{-2} mg/mL in CH_2Cl_2). This was accounted for by the increasingly close proximity of pyrene moieties between neighboring gold nanoparticles that favored the formation of pyrene excimers. It should be noted that the terminal pyrene groups in the long protecting ligands exhibited substantial freedom of movement, which led to face-to-face arrangements of the pyrene moieties from neighboring gold nanoparticles and consequently the formation

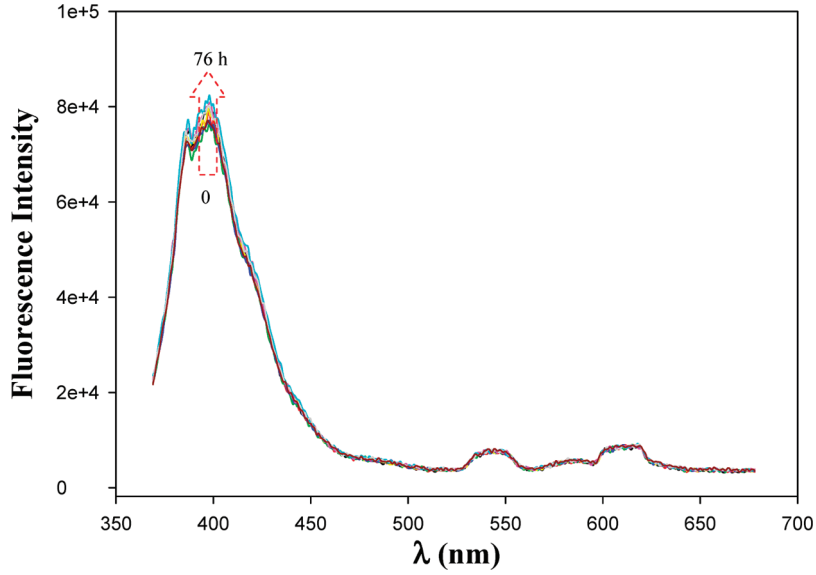

Figure 4. Fluorescence spectra of Ru═C8 nanoparticles mixed with 1-bromopyrene for varied periods of time (up to 76 h, as indicated by the red dashed arrow). Ru═C8 concentration, 0.01 mg/mL; 1-bromopyrene concentration, 3 mM. The excitation wavelength was 349 nm.

of excimers. Therefore, one may suspect that the emergence of a new emission peak at 490 nm with the Ru═VPy nanoparticles might also arise from the formation of pyrene excimers between neighboring nanoparticles. However, this is highly unlikely, because such an emission peak was absent with the Ru═APy nanoparticles, despite the same particle concentration and similar pyrene surface coverage. Additionally, a volcano-shape dependence of the fluorescence intensity on particle concentration was observed (Figure 2B), most probably due to fluorescence self-quenching by the nanoparticles, whereas the intensity of excimer emission typically increases monotonically with fluorophore concentration.[33] Furthermore, from the inset to Figure 2B, one can see that the 490 nm emission band becomes increasingly prominent with decreasing particle concentration, as compared to that at 392 nm. This is contradictory to the behaviors of excimers which are favored at high concentrations. Lastly, in these pyrene-functionalized Ru nanoparticles, the pyrene moieties were embedded within the protecting monolayer of much longer carbene ligands, rendering it difficult for the pyrene moieties to be close enough for the formation of excimers.

Taken together, the results presented above strongly suggest that, with a conjugated metal−carbene π bond, effective intraparticle conjugation occurs, leading to the appearance of a new emission peak in the lower energy region, whereas the incorporation of a saturated carbon spacer diminishes the electronic interactions between the fluorophores, and consequently the fluorophores behave independently.

The exchange reaction dynamics of Ru═C8 nanoparticles with vinylpyrene was then studied by monitoring the fluorescence profiles of a mixed solution of Ru═C8 particles (0.01 mg/mL) and vinylpyrene (3 mM) in DMF under vigorous stirring. Figure 3A depicts the emission spectra at different reaction times. At $t = 0$ h, the emission spectrum was essentially that of pyrene monomers with no feature at 490 nm. However, a new peak at 490 nm started to emerge and the peak intensity increased with increasing reaction times, suggesting the successful immobilization of pyrene moieties onto the nanoparticle surface by olefin metathesis reactions (the emission peak at 397 nm remained virtually invariant primarily because of the excess of monomeric vinylpyrene). After about 24 h, the fluorescence profile appeared to reach a steady state. Panel B depicts the variation of the emission peak intensity (at 490 nm) with time, where the symbols are experimental data collected from panel A and the solid line is the corresponding exponential fit. From the fit, the pseudo-first-order reaction rate constant was estimated to be 0.122 h^{-1}. Taking into account the concentration of vinylpyrene (3 mM), the corresponding second-order rate constant was evaluated to be 1.13×10^{-2} M^{-1} s^{-1}, which is highly comparable to that of metathesis reactions of Ru═C8 nanoparticles with 11-bromo-1-undecene.[8]

A comparative study was also carried out with Ru═C8 nanoparticles (0.01 mg/mL) and 1-bromopyrene (3 mM). Figure 4 shows the emission spectra acquired after the solution was mixed for different periods of time (up to 76 h). It can be seen that the fluorescence profiles remained practically unchanged, and consistent with that of pyrene monomers (Figure 2). This further confirms that the emission peak at 490 nm can only be ascribed to nanoparticle-bound pyrene moieties through Ru═C π bonds (of course, it also signifies that even at this pyrene concentration no excimer was formed).

The lifetimes (τ) of the fluorescence dynamics of the pyrene-functionalized ruthenium nanoparticles as well as the monomeric pyrene derivatives were then evaluated by nanosecond laser spectroscopy. Figure 5 depicts the fluorescence spectra acquired by using different gate widths (up to 160 ns) of (A) Ru═APy nanoparticles, (B) Ru═VPy nanoparticles, (C) a mixture of Ru═C8 nanoparticles and 1-bromopyrene, and (D) (*E*)-1,2-di(pyren-1-yl)ethene. As expected, it can be seen that overall the integrated fluorescence detected increases with increasing gate width. The time dependence of the fluorescence was then fitted by eq 1, from which the lifetime (τ) (or lifetimes if two were required to fit the data) of emission could be estimated. It should be noted that, for Ru═VPy and pyrene dimer, the dynamics curves exhibited a better fit by a biexponential equation with two different time constants corresponding to the two emission bands, whereas for other samples the data were fitted sufficiently well by a single exponential term. Table 1 summarizes the lifetimes (τ) for the pyrene derivatives as well as for the varied Ru nanoparticles. It can be seen that the lifetime of the 392 nm emission was the longest for allylpyrene (37 ns), which was longer than vinylpyrene possibly because it lacks the unsaturated side chain whose presence could contribute to nonradiative processes. The lifetime decreased somewhat when allylpyrene was attached onto the Ru nanoparticle surface

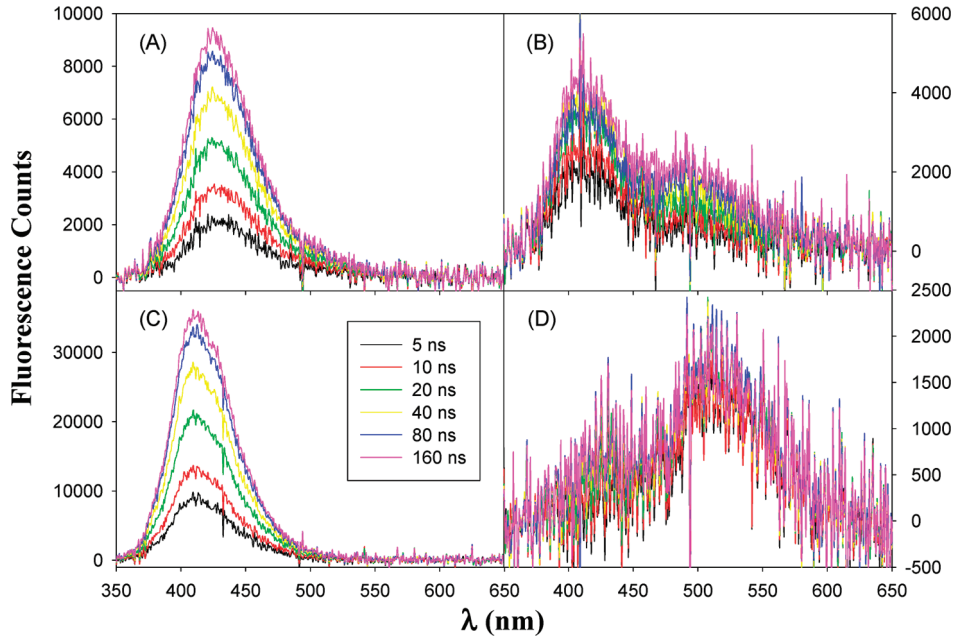

Figure 5. Nanosecond time-resolved fluorescence spectra of (A) Ru═APy nanoparticles, (B) Ru═VPy nanoparticles, (C) a mixture of Ru═C8 nanoparticles and 1-bromopyrene, and (D) (*E*)-1,2-di(pyren-1-yl)ethene (i.e., pyrene dimer). The gate widths were as specified in the figure legends.

TABLE 1: Lifetime (τ) of Fluorescence Emission of the Nanoparticles and Monomeric Pyrene Derivatives

τ (ns)	vinylpyrene	allylpyrene	pyrene dimer	Ru═VPy	Ru═APy	mixture of Ru═C8 and 1-bromopyrene
392 nm	26	37	17	7	29	25
490 nm			<5	62		

(Ru═APy, 29 ns, comparable to that measured with a simple mixture of Ru═C8 nanoparticles and 1-bromopyrene, 25 ns), possibly as a consequence of energy transfer from the pyrene moieties to the Ru nanocores. The decrease of fluorescence lifetime of the 392 nm emission was far more drastic when vinylpyrene (26 ns) was compared to the conjugated pyrene dimer (17 ns) or Ru═VPy nanoparticles (7 ns), which might be ascribed to the conjugated —CH═CH— spacer or Ru═carbene π bonds that facilitated electron as well as energy transfer between the pyrene moieties and the metal cores. It is interesting, however, that the lifetime of the 490 nm emission band varies significantly between Ru═VPy nanoparticles (62 ns) and the pyrene dimer (<5 ns). The neighboring organic protecting ligands may create a more rigid chemical environment for the nanoparticle-bound pyrene moieties and thus prolong the life of the excited state (Scheme 2), as compared to the strong electrostatic perturbations which exist in free solution when surrounded by a polar solvent. The long lifetime of the Ru═VPy nanoparticles may suggest that the nanoparticles are less prone to photobleaching possibly as a consequence of the prohibition of nonradiative decay processes.

Conclusion

Pyrene-functionalized ruthenium (Ru═VPy and Ru═APy) nanoparticles were prepared by olefin metathesis reactions of carbene-passivated nanoparticles with 1-vinylpyrene and 1-allylpyrene. The resulting particles exhibited unique optical properties. Specifically, their fluorescence properties were found to vary significantly with the structure of the chemical linker. For Ru═VPy nanoparticles, where the pyrene moieties were bound onto the nanoparticle surface directly by Ru═C π bonds, the fluorescence profile was consistent with that of pyrene dimer bridged by a conjugated spacer, with two prominent emission peaks at 392 and 490 nm. This suggests that, because of the metal−ligand π bonding interactions and consequently intraparticle extended conjugation, the particle-bound pyrene moieties behaved equivalently to conjugated pyrene dimers. In sharp contrast, when an sp^3 carbon was inserted into the chemical linker that bound the pyrene moieties onto the nanoparticles, the intraparticle extended conjugation was effectively turned off. This was manifested by Ru═APy nanoparticles which exhibited a fluorescence profile consistent with those of monomeric pyrene derivatives (vinylpyrene and allylpyrene). Furthermore, fluorescence dynamics studies showed that the Ru═VPy nanoparticles exhibited a much longer lifetime for the emission at 490 nm, implying that the particles might be less prone to photobleaching than conjugated pyrene dimers. Taken together, these results suggest that the optical characteristics of fluorophore-functionalized nanoparticles might be readily and effectively controlled by metal−ligand bonding interactions as well as the structure of the chemical linkages.

Acknowledgment. This work was supported in part by the National Science Foundation (CHE-0832065 and DMR-0804049) and the ACS-Petroleum Research Fund (49137-ND10).

Supporting Information Available: Detailed synthetic procedures for pyrene derivatives, NMR spectra of the organic components of the Ru═VPy and Ru═APy nanoparticles after the metal cores were dissolved by dilute KCN, and FTIR spectra of the Ru═VPy and Ru═APy nanoparticles and monomeric pyrene derivatives (1-vinylpyrene and 1-allylpyrene). This material is available free of charge via the Internet at http://pubs.acs.org.

References and Notes

(1) Templeton, A. C.; Wuelfing, M. P.; Murray, R. W. *Acc. Chem. Res.* **2000**, *33*, 27–36.
(2) Shenhar, R.; Rotello, V. M. *Acc. Chem. Res.* **2003**, *36*, 549–561.
(3) Caragheorgheopol, A.; Chechik, V. *Phys. Chem. Chem. Phys.* **2008**, *10*, 5029–5041.
(4) Mirkhalaf, F.; Paprotny, J.; Schiffrin, D. J. *J. Am. Chem. Soc.* **2006**, *128*, 7400–7401.
(5) Ghosh, D.; Chen, S. W. *J. Mater. Chem.* **2008**, *18*, 755–762.
(6) Ghosh, D.; Pradhan, S.; Chen, W.; Chen, S. W. *Chem. Mater.* **2008**, *20*, 1248–1250.
(7) Ghosh, D.; Chen, S. W. *Chem. Phys. Lett.* **2008**, *465*, 115–119.
(8) Chen, W.; Davies, J. R.; Ghosh, D.; Tong, M. C.; Konopelski, J. P.; Chen, S. W. *Chem. Mater.* **2006**, *18*, 5253–5259.
(9) Chen, W.; Chen, S. W.; Ding, F. Z.; Wang, H. B.; Brown, L. E.; Konopelski, J. P. *J. Am. Chem. Soc.* **2008**, *130*, 12156–12162.
(10) Chen, W.; Brown, L. E.; Konopelski, J. P.; Chen, S. W. *Chem. Phys. Lett.* **2009**, *471*, 283–285.
(11) Hush, N. S. *Electrochim. Acta* **1968**, *13*, 1005–1023.
(12) Kang, K. A.; Hong, B. N. *Crit. Rev. Eukaryotic Gene Expression* **2006**, *16*, 45–60.
(13) Bene, L.; Szentesi, G.; Matyus, L.; Gaspar, R.; Damjanovich, S. *J. Mol. Recognit.* **2005**, *18*, 236–253.
(14) Aguila, A.; Murray, R. W. *Langmuir* **2000**, *16*, 5949–5954.
(15) Sudeep, P. K.; Ipe, B. I.; Thomas, K. G.; George, M. V.; Barazzouk, S.; Hotchandani, S.; Kamat, P. V. *Nano Lett.* **2002**, *2*, 29–35.
(16) Brust, M.; Walker, M.; Bethell, D.; Schiffrin, D. J.; Whyman, R. *J. Chem. Soc., Chem. Commun.* **1994**, 801–802.
(17) Brown, L. O.; Hutchison, J. E. *J. Am. Chem. Soc.* **1999**, *121*, 882–883.
(18) Green, M.; Allsop, N.; Wakefield, G.; Dobson, P. J.; Hutchison, J. L. *J. Mater. Chem.* **2002**, *12*, 2671–2674.
(19) Kumar, A.; Mandal, S.; Selvakannan, P. R.; Pasricha, R.; Mandale, A. B.; Sastry, M. *Langmuir* **2003**, *19*, 6277–6282.
(20) Stapleton, J. J.; Daniel, T. A.; Uppili, S.; Cabarcos, O. M.; Naciri, J.; Shashidhar, R.; Allara, D. L. *Langmuir* **2005**, *21*, 11061–11070.
(21) Geiger, M. W.; Turro, N. J. *Photochem. Photobiol.* **1975**, *22*, 273–276.
(22) Ashikawa, I. N. Y.; Tsuboi, M.; Zama, M. *J. Biochem.* **1982**, *92*, 1425–1430.
(23) Tong, A. J.; Yamauchi, A.; Hayashita, T.; Zhang, Z. Y.; Smith, B. D.; Teramae, N. *Anal. Chem.* **2001**, *73*, 1530–1536.
(24) Corma, A.; Galletero, M. S.; Garcia, H.; Palomares, E.; Rey, F. *Chem. Commun.* **2002**, 1100–1101.
(25) Beer, P. D.; Gale, P. A. *Angew. Chem., Int. Ed.* **2001**, *40*, 486–516.
(26) Cumming, W. J. G., R. A.; Ingwall, R. T.; Kolb, E. S.; Mehta, P. G.; Minns, R. A. Polaroid Corporation: Cambridge, MA, U.S. Patent 5 414 069, 1995.
(27) Takuwa, A.; Kanaue, T.; Yamashita, K.; Nishigaichi, Y. *J. Chem. Soc., Perkin Trans. 1* **1998**, 1309–1314.
(28) Malashikhin, S.; Finney, N. S. *J. Am. Chem. Soc.* **2008**, *130*, 12846–12947.
(29) Geerts, J. P.; Martin, R. H. *Bull. Soc. Chim. Belg.* **1960**, *69*, 563–569.
(30) Hug, S. J.; Lewis, J. W.; Einterz, C. M.; Thorgeirsson, T. E.; Kliger, D. S. *Biochemistry* **1990**, *29*, 1475–1485.
(31) Szundi, I.; Lewis, J. W.; Kliger, D. S. *Biophys. J.* **1997**, *73*, 688–702.
(32) Benniston, A. C.; Harriman, A.; Lawrie, D. J.; Rostron, S. A. *Eur. J. Org. Chem.* **2004**, *227*, 2272–2276.
(33) Forster, T. *Angew. Chem., Int. Ed.* **1969**, *8*, 333–343.
(34) Mohanambe, L.; Vasudevan, S. *J. Phys. Chem. B* **2006**, *110*, 14345–14354.
(35) Wang, T. X.; Zhang, D. Q.; Xu, W.; Yang, J. L.; Han, R.; Zhu, D. B. *Langmuir* **2002**, *18*, 1840–1848.

JP906874F